

Article

Method for Unloading Zonation Based on Strain per Unit Crack: Case Study of a Large-Scale Rocky Slope on the Qinghai–Tibet Plateau

Zhengxuan Xu ^{1,2}, Guoqing Chen ^{3,*}, Xiang Sun ³, Xin Yang ³ and Zhiheng Lin ²

¹ Faculty of Geosciences and Environmental Engineering, Southwest Jiaotong University, Chengdu 610031, China

² China Railway Eryuan Engineering Group Co., Ltd., Chengdu 610031, China

³ State Key Laboratory of Geohazard Prevention and Geoenvironment Protection, Chengdu University of Technology, Chengdu 610059, China

* Correspondence: chgq1982@126.com

Abstract: Distribution of unloading zones determines stability of slopes, and the unloading of a large-scale rocky slope formed by rapid river erosion and surface uplift on the Qinghai–Tibet Plateau is particularly severe. Generally, unloading assessment relies on traditional methods, which are mainly related to phenomena. However, unloading is a process of deformation and failure regarding the rock mass. Based on deformation and failure, strain rate and crack rate established through theoretical analysis can measure the relationship between accumulative width of open cracks and unloading deformation and the relationship between accumulative number of cracks and unloading failure, respectively. Thus, a method that combines strain rate and crack rate, namely strain per unit crack (i.e., SPUC), is proposed. The SPUC was applied to assess the unloading zones of a large-scale rocky slope on the Qinghai–Tibet Plateau. The results show that the SPUC curve regularly varied and can be easily divided into three parts. Strong and weak unloading zones can be recognized from the SPUC curve. The reasonability of SPUC in the unloading zones assessment was confirmed by comparing and verifying with traditional methods. We found that SPUC has good universality and can compensate for the defect of using strain rate or crack rate to assess unloading zones.

Keywords: unloading zonation; large-scale rocky slope; Qinghai–Tibet Plateau; strain per unit crack

Citation: Xu, Z.; Chen, G.; Sun, X.; Yang, X.; Lin, Z. Method for Unloading Zonation Based on Strain per Unit Crack: Case Study of a Large-Scale Rocky Slope on the Qinghai–Tibet Plateau.

Sustainability **2023**, *15*, 3861.

<https://doi.org/10.3390/su15043861>

Academic Editors: Kaihui Li and Jianjun Ma

Received: 17 January 2023

Revised: 14 February 2023

Accepted: 18 February 2023

Published: 20 February 2023



Copyright: © 2023 by the authors. Licensee MDPI, Basel, Switzerland. This article is an open access article distributed under the terms and conditions of the Creative Commons Attribution (CC BY) license (<https://creativecommons.org/licenses/by/4.0/>).

1. Introduction

The Qinghai–Tibet Plateau, which is located at the junction with Eurasia and affected by continuous crustal uplift as well as stream trenching, has developed intensive structural activities and a tremendous number of active Holocene faults [1–4]. It has formed an enormous number of large-scale rocky slopes with strong unloading environments [5]. Unloading weakens the quality of rock mass [6–10], thereby affecting the stability of the slope [11–13]. Cracks formed by unloading are often the factor controlling slope stability in engineering, especially on large-scale rocky slopes [14,15], and many landslides are caused by unloading [16]. Therefore, quantifying distribution range of unloading zones is essential for structural safety in slope engineering.

Although many investigations have focused on unloading zonation, they are not unified in engineering, which leads to inconsistencies in the assessment methods and division indexes [17,18]. The previous methods can be classified into three categories: qualitative unloading zonation methods, quantitative unloading zonation methods, and auxiliary unloading zonation methods. Qualitative unloading zonation methods include division by geologists and division by the in situ stress field [19–22]. These methods are

mainly related to phenomena and depend on the experience of geologists. Quantitative unloading zonation methods include dividing by width of open cracks, gaps between fractures, rate of open cracks, rock quality indexes, fragmentation modulus, deformation modulus, etc. [23–28]. These methods are most widely used in engineering, but most of them are difficult to unify in different engineering slopes [29,30]. Auxiliary unloading zonation methods include dividing by longitudinal wave velocity and wave velocity ratio [31,32], apparent resistivity [33], permeability coefficient, Lyu Rong’s value [34–37] (Figure 1), radon gas anomaly [38–41], etc. These methods represent unloading but cannot eliminate weathering and other factors and require corresponding equipment to obtain them, which is technically more inconvenient.

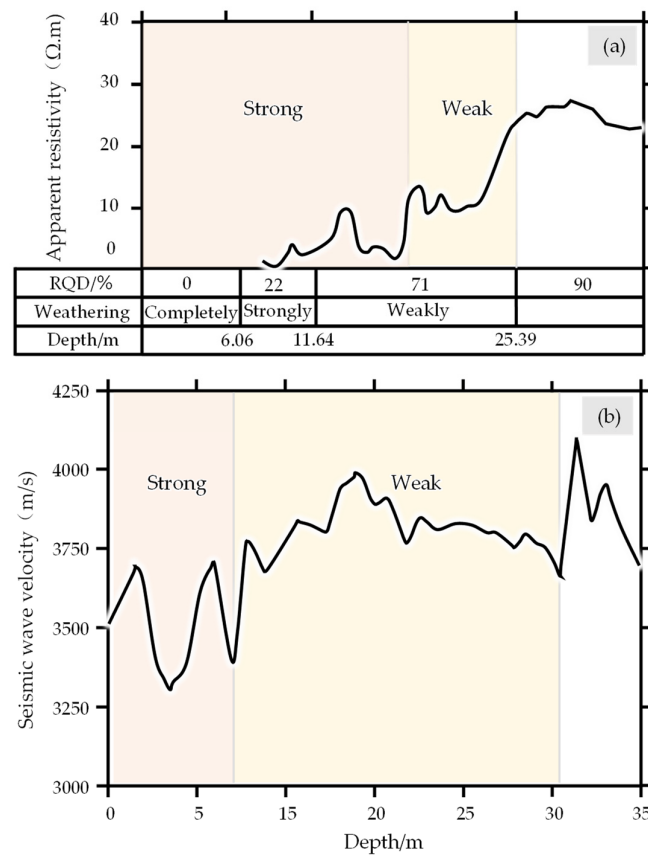


Figure 1. Examples of using various methods to divide the unloading zones. (a) Unloading zonation based on the rock quality designation (RQD) and apparent resistivity of the ZK127 borehole of the Three Gorges Project [36]. (b) Unloading zonation based on the seismic wave velocity at the high slope of the Three Gorges permanent ship lock [36].

Multiple indexes are most often used in unloading zonation, while the indexes used vary [36,42–45] (Table 1). Even for the same index, the criteria of division are different for various engineering slopes (Table 2). For instance, Lyu Rong’s values of the lower boundary of the strong and weak unloading zones of Tongjiezi basalt are 100 Lu and 5 Lu, respectively [46], while they are 100 Lu and 1 Lu, 100 Lu and 10 Lu, and 10 Lu and 1 Lu for Xiaowan Hydropower Station [47], Laxiwa Hydropower Station [48], and Baihetan Hydropower Station [49], respectively. In addition, the unloading zonation index of Goupitan Hydropower Station is an elastic wave velocity of 4000 m/s, while that of Dongfeng Hydropower Station is 5000 m/s. However, the exclusive lithology of both areas is limestone. Due to the differences in methods and engineering backgrounds, there is no agreement on unloading zonation, which is not conducive to popularization and

application of quantitative indexes for assessing unloading zonation. Thus, developing a universal and easy-to-operate unloading assessment method is urgent.

Table 1. In different projects, unloading zonation usually adopts multiple indexes, but the indexes used are different [36,42–45].

Hydropower Station	Lithology	Unloading Zonation Index
Xiaowan	Granite	Longitudinal wave velocity, fracture opening width
Longkaikou	Basalt	Longitudinal wave velocity
Xiluodu	Basalt	Longitudinal wave velocity, rock mass integrity coefficient
Baihetan	Basalt	Fracture opening width, fracture spacing, longitudinal wave velocity, number of fracture openings, unit gap width, and unit number of fractures
Jinping	Marble, sandstone, slate	Fracture opening width, fracture spacing, longitudinal wave velocity
Xiangjiaba	Sandstone	Number of fractures, fracture opening width
Pubugou	Basalt, granite	Longitudinal wave velocity
Yangfanggou	Granodiorite	Fracture rate, fracture opening width
Guandi	Dolomite, sandstone, shale	Longitudinal wave velocity
Dagangshan	Granite, diorite	Fracture opening width, types of rock mass structures, longitudinal wave velocity

Table 2. When the same index is used in unloading zonation, the standards used in different projects are different [36].

Hydropower Station	Lithology	Main Characteristics of Strong Unloading Zones		Range/m
		Crack Width/cm	Elastic Wave Velocity/(m·s ⁻¹)	
Wudongde	Marble	1.0–5.0	3400–3600	0–18
Tacheng	Phyllite	0.5–2.0	2800–3500	0–36
Three Gorges	Granite	0.5–1.0	3300–3600	0–8
Permanent Shiplock				
Jinping I	Hypometamorphic rock	3.0–7.0	≤3800	5–20
Xiaowan	Metamorphic rock	>2.0	≤3000	7–34
Xiluodu	Basalt	>2.0	≤3000	5–15
Baihetan	Basalt	2.0–15.0	2100–3400	0–54
Guandi	Basalt	1.0–10.0	≤2000	7–53

The nature of unloading involves rebound of the rock mass driven by erosion of valleys or artificial excavation [50,51]. Its engineering geological characteristics are mainly manifested as spring-back loosening, shear dislocation, and new cracks in the rock mass (i.e., deformation and failure) [52,53]. Therefore, strain per unit crack (SPUC), which combines the strain rate and crack rate of the rock mass, was proposed to quantitatively divide the unloading zones. SPUC was applied to assess the unloading zones of a large-scale rocky slope on the Qinghai–Tibet Plateau. Considering the nature of unloading and combining strain rate and crack rate, zoning based on an abrupt change in the SPUC curve is uniform and can avoid the shortcomings of insufficient evaluation of the rock mass quality by using strain rate and insufficient evaluation of the rock mass strain degree by using crack rate.

2. Study Area

2.1. Geological Setting

The study area is situated in Baiyu County, Ganzi Tibetan Autonomous Prefecture, Sichuan Province, China. The study area is located on the eastern margin of the Qinghai–Tibet Plateau, which is called the Jiarishan slope (JRS) (Figure 2). Jiangqu River, a tributary of Jinsha River, passes through the foot of the JRS, with a water surface elevation range of 3170 m to 3200 m, and it flows to the northwest. The valley of the Jinsha River reach in this region is a typical erosional valley. This deep canyon landform, affected by river cutting, forms a strong unloading environment. The relative height difference is 1331 m, showing a steep downward and gentle upward trend, with a slope of approximately 35° (Figure 3).

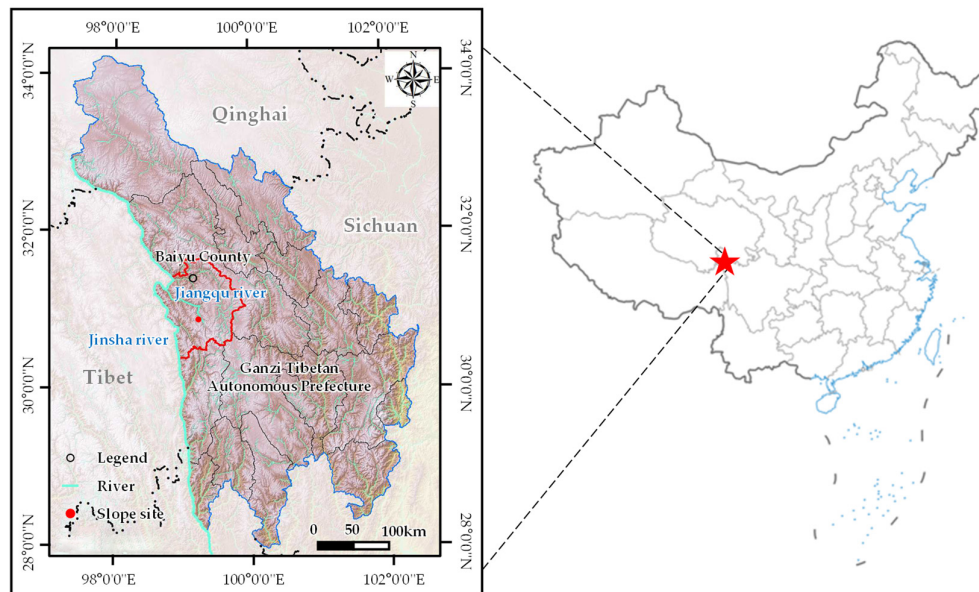


Figure 2. Map showing the location of the JRS.

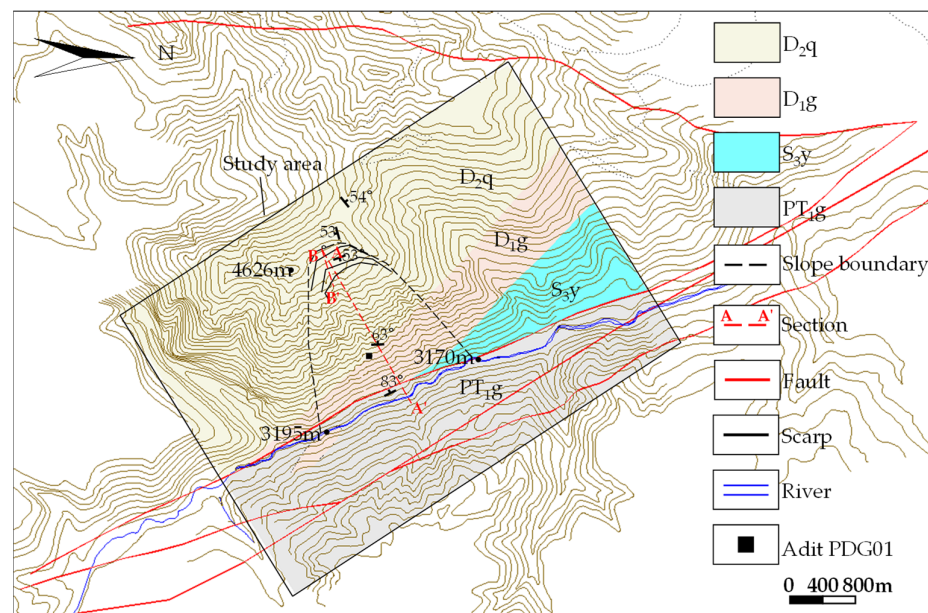


Figure 3. Engineering geological planar graph of the study area.

The exposed layer of the slope is mainly composed of carbonaceous crystalline limestone and argillaceous dolomite of Silurian Yongren Formation (S_{3y}). The surface weathering is grayish-white, with a single-layer thickness of 20 cm to 100 cm. Devonian Gerong Formation (D_{1g}) consists of massive light-yellow dolomite and dolomitic limestone. Devonian Qiongcuo Formation (D_{2q}) contains thick massive crystalline limestone, biological limestone, fine-grained dolomite, dolomitic limestone, and a small amount of argillaceous limestone and shale. The thickness of a single layer is greater than 50 cm. The strata are oriented N20°–50°W/SW \angle 55°–70°. The residual slope overburden (Q_{4^{dl+el}}) is above the slope surface elevation of 4418 m, and the collapsed slope overburden (Q_{4^{col+dl}}) is below the slope surface elevation of 3600 m, which is mainly composed of crushed stone, and the overburden thickness is generally 5 m to 20 m (Figure 4a, Table 3). The lithologies exposed by the slope are mainly limestone and dolomite, which are hard rock masses. They can store substantial elastic potential energy and are more conducive to springing back during unloading. In addition to the deep river valley, steep bank slope, large slope elevation difference, freeze–thaw karst development, and long unloading time, the unloading environment of the slope is strong and complex.

Table 3. Stratigraphic units and lithological characteristics on the slope area.

Strata	Main Lithology	Thickness/m	Cardinal Features	
			Stratified Structure	Hardness
S _{3y}	Crystalline limestone and argillaceous dolomite	20–100	Thick	Hard
D _{1g}	Dolomite and dolomitic limestone	>50	Thick	Hard
D _{2q}	Crystalline limestone	>50	Thick	Hard
Q _{4^{dl+el}}	Crushed stone and Silty clay	5–10	/	/
Q _{4^{col+dl}}	Crushed stone	10–30	/	/

The study area is located in the western wing of the Nawa–Yuci syncline. At the foot of the slope, the NNW-trending Jiangqu fault is distributed along Jiangqu River, and its occurrence is N20°–30°W/SW \angle 55°–70° (Figure 3). The fault was active in the early Pleistocene to middle Pleistocene, and its activity has been weak since the late Pleistocene [54].

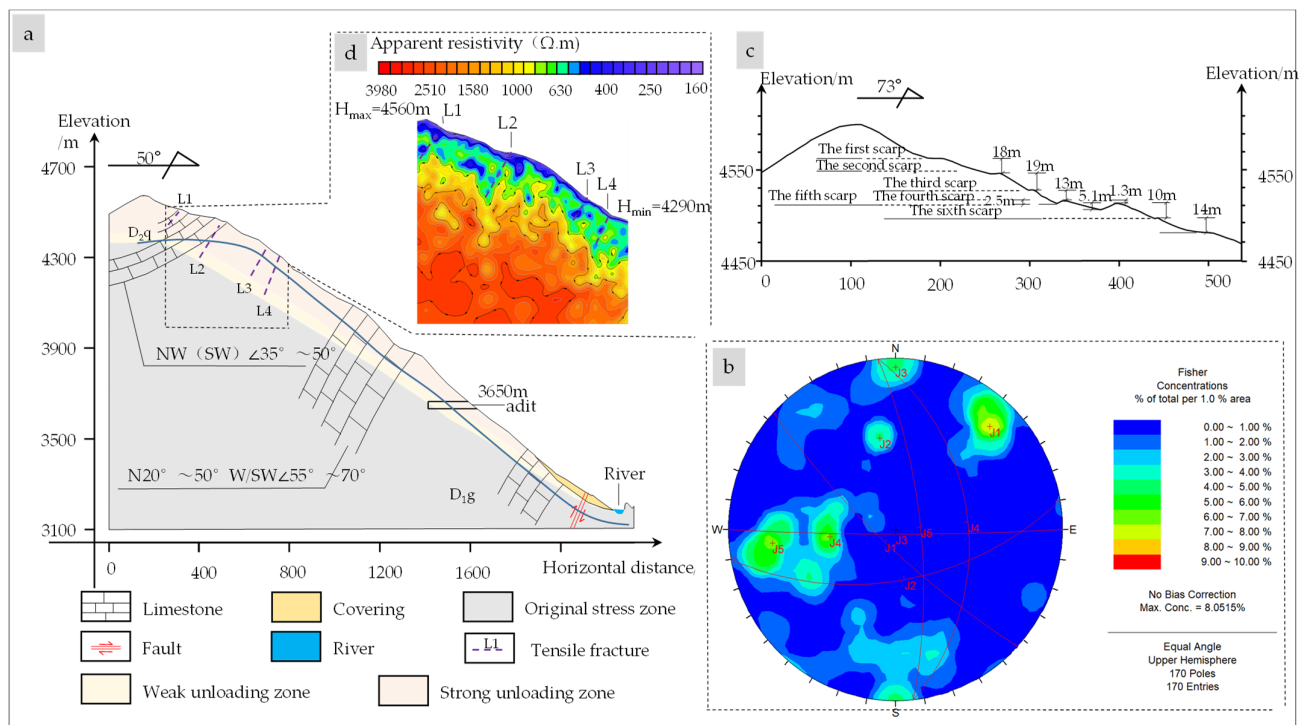


Figure 4. (a) Engineering geological profile of the study area. (b) Contour diagram of poles for the main structural planes in adit PDG01. (c) Engineering geological profile of the scarps. (d) Dissolution cavities are visible in the resistivity test results of the slope crest.

2.2. Field Investigation

The constructor of a railway project built one horizontal adit, namely PDG01, on the JRS, which is shown in Figures 3 and 4a, to study the structural characteristics of the rock mass from the surface to the inside to help divide the unloading zones. The characteristics and structure of the rock mass in PDG01 have been observed.

Horizontal adit PDG01 is located on the left bank of Jiangqu River at an elevation of 3650 m. It has a strike of N65°E with a length of 200 m and a cross-section size of 2 m × 2 m. The main stratum exposed in adit PDG01 is D_{2q}. The main cracks, including large discontinuities, rock layers, faults, and compressional shear zones, which developed in the three walls (right sidewall, left sidewall, and roof) of adit PDG01, are presented in Figure 5.

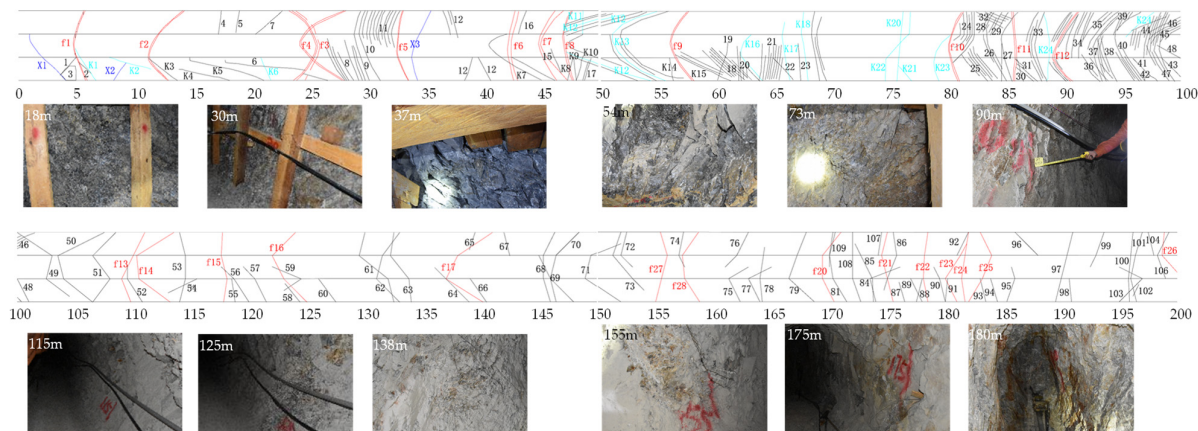


Figure 5. Distribution of cracks development in PDG01 (Black lines represent normal cracks, red lines represent faults, and cyan lines represent dissolution cracks).

As a statistical result, five predominant groups of large discontinuities, which are hard discontinuities with lengths greater than 2 m, are formed in adit PDG01 and have occurrences of N35°–60°W/NE \angle 71°–88°, N70°–80°E/NW \angle 50°–60°, EW/N \angle 80°–90°, N5°–20°E(W)/NW(SW) \angle 35°–50°, and N5°–20°E(W)/NW(SW) \angle 60°–85° (Figure 4b), and the first group is the best developed. Twenty-six small faults are developed in the section 0–200 m away from the entrance of adit PDG01. All twenty-six small faults have lengths of 5 to 100 m and thicknesses of 1 to 30 cm. They are divided into intrastee slopes and laterally steep slopes (f3, f15, f24, and f25).

Due to the serious weathering and unloading of the slope, the number of cracks is too large to carry out comprehensive statistics; thus, detailed field measurements are carried out on cracks with extension lengths of more than 2 m in adit PDG01, and the number of cracks and width of open cracks are counted (Table 4). In short, 0–50 m is the distribution area of the cataclastic loose rock mass, which is supported in adit PDG01; thus, the statistics of cracks are incomplete.

Table 4. Characterization of main cracks in adit PDG01.

Depth/ m	Number of Cracks per 5 m	Width of Open Cracks per 5 m/cm	Depth/m	Number of Cracks per 5 m	Width of Open Cracks per 5 m/cm
0–5	3	3.5	100–105	3	0.3
5–10	4	3.8	105–110	4	1.0
10–15	1	1.0	110–115	2	0.1
15–20	4	7.3	115–120	2	0.0
20–25	3	15.5	120–125	4	0.0
25–30	10	2.5	125–130	3	0.0
30–35	9	1.0	130–135	6	0.5
35–40	5	1.5	135–140	4	0.5
40–45	5	4.0	140–145	1	0.0
45–50	13	12.4	145–150	4	0.5
50–55	1	1.0	150–155	3	0.0
55–60	2	4.0	155–160	2	0.0
60–65	25	10.4	160–165	4	0.5
65–70	7	14.0	165–170	1	0.0
70–75	1	3.0	170–175	6	0.7
75–80	4	13.0	175–180	6	0.5
80–85	25	3.2	180–185	4	1.3
85–90	9	7.7	185–190	2	0.0
90–95	22	0.0	190–195	3	0.3
95–100	27	1.2	195–200	6	0.1

Field investigation revealed that the top of the slope was developed at seven levels of scarps, among which the height difference between the fourth level scarp and the fifth level scarp was small, only 1 m to 2 m. In addition, except for the first level scarp, the surfaces of other scarps had obvious grooves with depths ranging from 0.3 m to 5 m, among which the trailing edge of the fifth level scarp had the largest depth of approximately 5 m (Figure 4c). Therefore, we only determined the resistivity measurement of the top area in the 4290 m to 4560 m zone and not the resistivity measurement of the entire slope; the resistivity changes in the range of 200–3980 Ω . The deep areas suddenly decrease, but the overall performance increases (Figure 4d).

3. Methods

Unloading is the process of energy release, which is accompanied by deformation and failure of the rock mass. Therefore, the extent of unloading can be quantified if deformation and failure are quantified. Deformation and failure of the rock mass caused by energy release can be measured by strain rate and crack rate, respectively.

Strain rate is proposed according to energy superposition statistical theory of the rock structure, which considers that the energy released during the unloading process can be approximately regarded as the sum of the energy released by the rock block and the energy released by cracks (Figure 6). After simplification, strain rate can be expressed by the changing rate of the accumulative width of open cracks with depth (Δh - ε curve). The following is the simplest case to explain the strain rate method used in unloading zonation. Only the relationship between strain energy and width of open cracks in the statistical theory of rock structure under uniaxial tensile conditions is most thoroughly explained. For details, refer to Wu et al. [26,55,56] and Bao et al. [30].

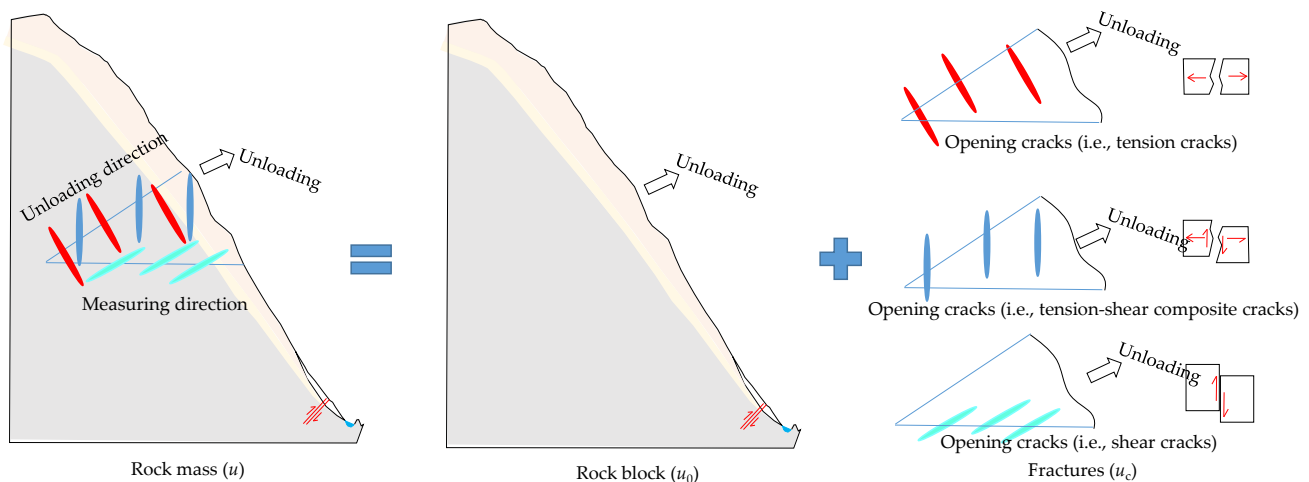


Figure 6. The energy released in the unloading process can be approximately regarded as the sum of the energy released by the rock block and the energy released by cracks. Cracks include open cracks and closed cracks (i.e., tension cracks, tension-shear composite cracks, shear cracks).

According to the statistical theory of rock mass structure, the strain energy density generated and stored by any rock mass element under the action of stress σ_{ij} is expressed as Equation (1).

$$u = u_0 + u_c \quad (1)$$

where u_0 and u_c are the strain energy density caused by the rock block and cracks, respectively.

When the rock mass undergoes elastic unloading, Equation (1) reflects the strain energy density u released by the rock mass under the action of the unloading stress σ_{ij} , which can be expressed as Equation (2).

$$u = u_0 + u_c = \frac{1}{2} \sigma_{ij} C_{oijkl} \sigma_{kl} + \frac{1}{2} \sigma_{ij} C_{cijst} \sigma_{st} \quad (2)$$

According to the elasticity, C_{oijkl} can be expressed as Equation (3).

$$C_{oijkl} = \frac{1+\mu}{2E} (\delta_{ik} \delta_{jl} + \delta_{il} \delta_{jk}) - \frac{\mu}{E} \delta_{ij} \delta_{kl} \quad (3)$$

When considering that cracks in unloading rock masses are mostly open cracks and have no water, C_{cijst} can be expressed as Equation (4) [26,55,56].

$$C_{cijst} = \frac{16(1-\mu^2)}{\pi E} \sum_1^m \lambda \bar{a} \left[\left(1 - \frac{2}{2-\mu}\right) n_i n_j n_s n_t + \frac{2}{2-\mu} \delta_{ij} n_j n_s \right] \quad (4)$$

where C_{oijkl} , C_{cijst} , E , μ , λ , m , \bar{a} , δ_{ij} , σ_{ij} , and n_i are the fourth-order elastic compliance tensor of rock blocks, the fourth-order compliance tensor of cracks, the elastic modulus, Poisson's ratio, the normal density of a set of cracks, number of crack sets, mean radius of a set of cracks, second-order unit tensor, stress tensor, and the cosine of the included angle between the direction of tensile stress and the crack normal, respectively.

More specifically, if unloading is considered to add tensile stress σ in a certain direction, it becomes a form of uniaxial tension according to the statistical theory of rock mass structure. In particular, when the unloading force acting along the normal direction of a set of cracks causes only the group of structural planes to open and the existence of other groups of cracks can be ignored, then the strain energy density caused by this tensile stress can be expressed as Equation (5).

$$u = \frac{1}{2} \sigma \left[\frac{1}{E} + \frac{16(1-\mu^2)}{\pi E} \lambda \bar{a} \right] \sigma \quad (5)$$

According to fracture mechanics, the mean radius of this set of cracks, \bar{a} , can be expressed as Equation (6).

$$\bar{a} = \frac{3\pi E}{16(1-\mu^2)\sigma} \bar{t} \quad (6)$$

Substituting Equation (6) into Equation (5), another expression of the strain energy density, Equation (7), can be obtained.

$$u = \frac{1}{2} \sigma \left(\frac{\sigma}{E} + 3\lambda \bar{t} \right) = \frac{1}{2} \sigma \varepsilon_0 + \frac{3}{2} \sigma \lambda \bar{t} \quad (7)$$

where \bar{t} and ε_0 are the mean width of a set of open cracks and the unloading strain of the rock block, respectively.

The first part is the strain energy density released by the rock block, and the second part is the strain energy density released by cracks in Equation (7). If it is considered that the rebound deformation of the rock block is limited and the cracks may often be wide open, then the strain energy density released by the rock block is much smaller than that released by cracks. Therefore, the strain energy density and the unloading strain according to the statistical theory of rock mass structure can be expressed as Equations (8) and (9).

$$u \approx \frac{3}{2} \lambda \bar{t} \sigma \quad (8)$$

$$\varepsilon = \frac{\partial u}{\partial \sigma} \approx \frac{3}{2} \lambda \bar{t} = \frac{3}{2} \frac{\Delta n}{\Delta h} \bar{t} = \frac{3}{2} \frac{\sum \bar{t}_i}{\Delta h} \quad (9)$$

where Δn is the number of open crack noodles within the depth range of Δh and ε is the total unloading strain.

This means that, if the elastic deformation of the rock block is ignored and cracks are usually open, then the changing rate of accumulative width of open cracks with the depth (Δh - ε curve) constitutes the main body of the unloading strain. Therefore, as long as the accumulative width of open cracks with depth can be obtained, the unloading zones can be divided according to the derivative of the accumulative width of open cracks (i.e., the strain rate). Wu et al. [26] took the Xiaowan Hydropower Station as an example by using the strain rate obtained by borehole TV to describe the changes in the degree of unloading opening deformation in the sections. With the abrupt change point as the boundary, three

regions were divided into strong unloading zone, weak unloading zone, and original rock mass zone.

The index of the width of open cracks commonly used in engineering is similar to the strain rate. They both reflect the changes in the degree of unloading by measuring the strain caused by unloading. The strain rate has a clear physical meaning for unloading, and it is more convenient to operate to divide the unloading zones by the sudden change in the $\Delta h-\varepsilon$ curve as it has universal applicability.

Use of the strain rate to divide the unloading zone will lead to insufficient measurement of the rock mass quality. There are some defects in actual engineering when using strain rate to divide unloading zones. First, there are many cracks, but few of them are open cracks after the rock is broken by unloading in some locations, which leads to a quite low unloading strain rate. In addition, two sections with the same strain rate show the same opening with different crack numbers; one section has more closed cracks, while the other does not (Figure 7a). Therefore, when the number of closed cracks is relatively large and the unloading zone is divided by strain rate, adit sections with completely different rock mass structures will be classified into the same unloading zone, which is not perfect for engineering. In summary, the strain rate can only be applied alone to analyze the unloading zone if most cracks are open.

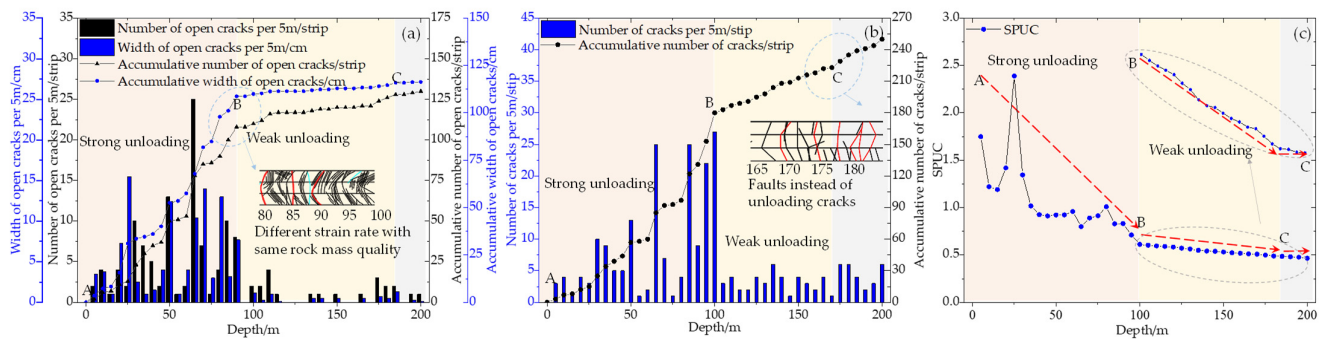


Figure 7. (a) Schematic diagram of the result of using the strain rate to divide the unloading zones ($\Delta h-\varepsilon$ curve). The results of unloading zonation by the number of open cracks. The results of dividing the unloading zones by the width of open cracks. (b) Schematic diagram of the result of using the crack rate to divide the unloading zones ($\Delta h-N_s$ curve). The results of unloading zonation by the number of cracks. (c) Schematic diagram of the result of using SPUC to divide the unloading zones ($\Delta h-SPUC$ curve).

The cracks are not always mostly open, and using the strain rate to divide the unloading zones will lead to inaccuracy in evaluation of the rock mass structure. However, the crack density and structural characteristics of rock masses can be reflected by the crack rate.

The strain rate is used to measure the strain caused by unloading, and the crack rate is used to measure the rock mass quality. Similar to calculation of strain rate (i.e., the strain of the rock block is ignored and only the strain generated by the structural plane is considered), only the macrocracks (i.e., the structural planes) are considered and the microcracks are ignored in calculation of crack rate, which is used to measure the rock mass. Therefore, the crack rate D is defined as the rate of the cumulative number of cracks N_s with depth (Δh), which is shown in Equation (10).

$$D = \frac{dN_s}{d\Delta h} \quad (10)$$

To facilitate operation in practical applications, failure of the rock block is ignored. That is, the changing rate of the accumulative number of cracks with depth ($\Delta h-N_s$ curve) constitutes the main body of the crack rate. Therefore, as long as the accumulative number of cracks with depth can be obtained, the unloading zones can be divided according to the

derivative of the accumulative number of cracks, that is, the slope of the Δh - N_s curve. This is the method of assessing unloading zones by crack rate.

When crack rate is used to divide the unloading zones, a disadvantage similar to the strain rate also appears. For instance, with the same number of crack groups but different openings, it is divided into the same unloading zone when using the crack rate for division, which is unreasonable. In addition, it cannot remove the effects of nonunloading cracks (e.g., faults) (Figure 7b). However, the strain rate and crack rate with clear physical meaning can complement the deficiencies of each other; thus, we averaged the degree of opening of each crack, including the closed cracks. The degree of unloading is characterized by the degree of opening of the unit crack. In this way, the strain rate can avoid insufficient characterization of rock mass quality. Therefore, based on the strain rate and crack rate, SPUC was defined for unloading zonation to compensate for their respective deficiencies. For the strain rate in Eq. 6, only the number of open cracks was considered; strain per unit crack, SPUC, was expressed as Equation (11).

$$SPUC = \frac{\varepsilon}{N_s} = \frac{3\bar{\lambda}t}{2N_s} = \frac{3\Delta n\bar{t}}{2N_s\Delta h} = \frac{3}{2} \frac{\sum \bar{t}_i}{N_s\Delta h} \quad (11)$$

where N_s is the cumulative number of cracks within the long depth range of Δh .

The unloading zones of the slope rock mass can be divided according to the slope of the Δh -SPUC curve, and the method of division is similar to that of the strain rate. Use of SPUC and Δh -SPUC curves to divide the unloading zones can prevent the shortcomings of insufficient characterization of the strain rate of rock mass quality and the defect of insufficient characterization of the strain for dividing the boundaries where cracks develop continuously. Dividing the unloading zones according to SPUC and verifying it by conventional means can make the results more scientific and feasible.

4. Results and Comparison

First, we used strain rate and crack rate to divide the unloading zones separately. When determining the strain rate (that is, the slope of the Δh - ε curve), it is temporarily included in the average interval consideration (Figure 7a), and the turning point position of the curve is determined accordingly. The strain rate of segment AB is significantly larger than that of segment BC, and the strain rate of segment BC changes less than that after point C. According to the strain rate, segment AB (0 m to 90 m) is classified as the strong unloading zone and segment BC (90 m to 185 m) is classified as the weak unloading zone.

Similar to strain rate, number of open cracks and width of open cracks both reflect degree of strain of the rock mass, and they have the same change trend. Figure 7a shows the statistics of the number of open cracks and the width of open cracks in adit PDG01. Note that the interval from 0 m to 50 m is the distribution area of the broken and loose rock mass. Due to the support in the adit, the statistics of cracks in this section are incomplete. In the interval from 50 m to 90 m, open cracks are widely developed, and the number of open cracks and width of open cracks are large. The number of open cracks is generally more than five, and the maximum is twenty-five in this section. The width of open cracks per 5 m is generally greater than 8 cm in this section. In the interval from 90 m to 185 m, the cracks mainly show micro-openings and closings, and the width of the open cracks is approximately 0.3 cm. The number of open cracks in this section decreases significantly, with approximately three open cracks showing a significant decreasing trend. Therefore, according to the number of open cracks and width of open cracks, segment AB (0 m to 90 m) is classified as the strong unloading zone and segment BC (90 m to 185 m) is classified as the weak unloading zone, which is the same as the result of the strain rate.

Based on analysis of accumulative number of cracks with depth (Δh - N_s curve), the crack rate, namely the slope of the Δh - N_s curve, is used to divide the unloading zones (Figure 7b). The crack rate of segment AB is significantly larger than that of segment BC,

and the crack rate of segment BC changes less than that after point C. Thus, segment AB (0 m to 100 m) is classified as the strong unloading zone and section BC (100 m to 170 m) is classified as the weak unloading zone.

Similar to crack rate, number of cracks measures degree of rock mass quality, and their changes have the same trend. Figure 7b shows the statistics of the number of cracks in adit PDG01. In the interval from 50 m to 100 m, the number of cracks is large. The number of cracks is generally more than ten, and the maximum is twenty-six. A comparison of the number of cracks with the number of open cracks reveals that most of the cracks in this section are opening. In the interval from 100 m to 170 m, the number of cracks in this section decreases significantly, with approximately five cracks showing a significant decreasing trend. Therefore, according to the number of cracks, a depth of 100 m can be classified as the lower limit of the strong unloading zone and a depth of 170 m can be classified as the lower limit of the weak unloading zone, which is the same as the result of the crack rate.

Comparison of the two partition results reveals that the reason for the obvious difference in the partition results is that strain rate does not consider rock mass quality; thus, the 80 m to 100 m adit section with the same obvious crack density is divided into two different regions (Figure 7a). In addition, this is obviously unreasonable. The crack rate is due to the influence of cracks only. After point C, the crack rate increases because there are more small cracks in the adit section of 170 m to 185 m, which are not caused by unloading but by fault (Figure 7b). However, this problem cannot be avoided by using the division of the crack rate only.

Thus, we combine the two methods and propose a method, i.e., SPUC, to reasonably divide the unloading zones (Figure 7c). The Δh -SPUC curve shows that the unloading of section AB is obviously larger than that of section BC, and the unloading of section BC and the unloading after point C change little. According to SPUC, section AB (0 m to 100 m) is a strong unloading area and section BC (100 m to 185 m) is a weak unloading area. Obviously, SPUC can avoid dividing the 80 m to 100 m adit section with the same obvious crack density into two different regions and over-measuring the rock mass quality.

5. Verification

According to the history of the regional geomorphic evolution, the slope model of the river valley is established in combination with the profile, and slope downcutting is simulated through discrete element software, which can consider the rock structure, such as layers and joints, to obtain the in situ stress distribution map of the slope [5].

The parameters used in the numerical simulation are obtained according to the experiments, as shown in Table 5, where ρ , E , μ , G_M , η_M , G_K , η_K , c_0 , c_r , φ_0 , φ_r , σ_{t0} , ε_r^{ps} , and ε_r^{pt} are density, elastic modulus, Poisson's ratio, shear moduli of the Maxwell body, viscosity coefficient of the Maxwell body, shear moduli of the Kelvin body, viscosity coefficient of the Kelvin body, initial cohesion, residual cohesion, initial internal friction angle, residual friction angle, initial tensile strength, shear plastic strain threshold, and tensile plastic strain threshold [57].

The boundary conditions of the model are the displacement constraint and velocity constraint at the bottom and the tectonic stress field that increases linearly with depth at both sides of the model [57].

Then, the bottom boundary of the unloading zone is determined according to the range of the stress reduction zone (Figure 8a,b).

Table 5. Parameters used in the numerical simulation.

Type	$\rho/(\text{kg}\cdot\text{m}^{-3})$	E/GPa	μ	G/GPa	$\eta/\text{GPa}\cdot\text{d}$	G_k/GPa	$\eta_k/\text{GPa}\cdot\text{d}$
Rock mass	2650	14	0.25	5.6	11.2	3.36	56
Fault	2200	4	0.35	1.48	2.96	1.18	14.8
Type	c_0/MPa	c_r/MPa	$\varphi_0/(\circ)$	$\varphi_r/(\circ)$	σ_0/MPa	ε_r^{ps}	ε_r^{pt}
Rock mass	1.5	0.3	55.0	30	1.2	0.02	0.001
Fault	0.1	0.1	30	30	0.0	0.02	0.001

The resistivity results are used to verify the rationality of using the in situ stress field. The area for determining the maximum resistivity value as the rock resistivity skeleton is $\rho_r = 3980 \Omega\cdot\text{m}$. The area and determination of the fracture zone (including the corrosion fracture zone) resistivity, as in the weak rock mass medium resistivity, is $\rho_w = 630 \Omega\cdot\text{m}$. It can be calculated according to the evaluation parameters and methods for tunnel engineering rock mass integrity proposed by Hua et al. [58]. When the measured resistivity average is less than $1000 \Omega\cdot\text{m}$ and K_r is 0.20 or less, it is the lower limit of the strong unloading zone. When the measured resistivity average is less than $1580 \Omega\cdot\text{m}$ and K_r is 0.50 or less, it is the lower limit of the weak unloading zone.

$$K_r = \frac{\Delta h_1}{\Delta h_1 + \Delta h_2} = \frac{\rho_r(\rho_{\text{mass}}^2 - \rho_w^2)}{\rho_r(\rho_{\text{mass}}^2 - \rho_w^2) + \rho_w(\rho_r^2 - \rho_{\text{mass}}^2)} \quad (12)$$

where ρ_{mass} , ρ_r , ρ_w , K_r , Δh_1 , and Δh_2 are resistivity of rock mass, resistivity of rock skeleton, resistivity of weak medium in the rock, rock mass integrity factor, thickness of rock skeleton, and thickness of the weak medium in the rock, respectively.

Combined with the apparent resistivity and gradient distribution, the unloading zones of the slope were divided, and the distribution of the unloading zones on the profile was obtained, as show in Figure 8b,c. Due to the long unloading time at the top of the slope, the horizontal unloading depth is obviously deeper than that of adit PDG01. The horizontal depth of the strong unloading bottom is approximately 200 m and that of the weak unloading bottom is approximately 250 m. This result is consistent with the results obtained by using the stress zones corresponding to the unloading zones. Finally, the lower limit of the weak unloading zone obtained by the method of dividing the unloading zone according to the in situ stress is 185 m at the elevation of adit PDG01.

In addition, the unloading zones can also be divided according to qualitative analysis (GB50487-2008, [19]) (Table 6). According to the geological survey and exploration of the adit, there is no large controlled active fault in the slope area, and the rock mass is dominated by joint cracks, while unloading cracks and dissolution cracks are developed in local sections. According to the field investigation (Figure 5 and Table 4), the interval of 0 m to 100 m can be classified as the strong unloading zone and the interval of 100 m to 185 m can be classified as the weak unloading area. The results of the new method are similar to the results obtained by the specification and the results obtained by in situ stress, and the slope unloading area can be reasonably evaluated according to SPUC (Table 7).

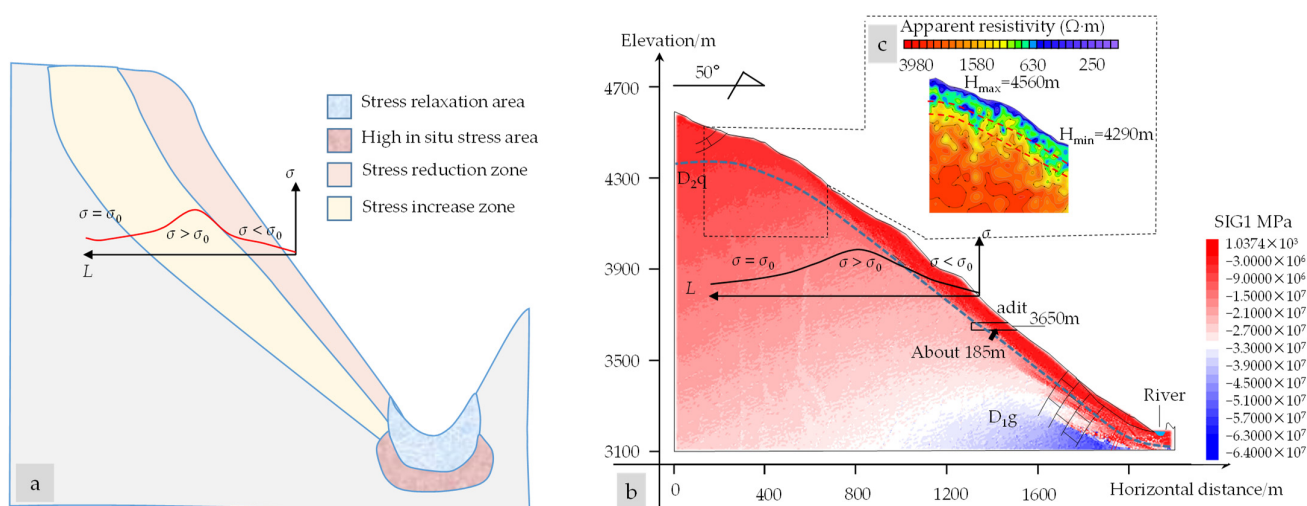


Figure 8. (a) Unloading zonation by using the stress field. (b) In discrete element software, the bottom boundary of the unloading zone is 185 m when the in situ stress is used to divide the unloading zones. (c) Resistivity is used to divide the unloading zones.

Table 6. Specification for geological investigation of water conservancy and hydropower engineering (Appendix J) and qualitative division of the rock unloading zone (part of the table).

Unloading Zones	Main Geological Characteristics
Strong	<ol style="list-style-type: none"> 1. The unloading cracks are densely developed and generally open. 2. The openings are generally a few centimeters to tens of centimeters. 3. Some have obvious loosening or displacement.
Weak	<ol style="list-style-type: none"> 1. The unloading cracks are sparsely developed. 2. The openings are generally a few millimeters to a few centimeters. 3. Most of the unloading fractures open along the original structural plane, and the rock mass is partially relaxed.

Table 7. Comparison of division results by using various unloading zonation methods.

Division Method	Strong Unloading Zones/m (Differences/%)	Weak Unloading Zones/m (Differences/%)
In situ stress	/(/)	185 (0)
Resistivity (top of slope)	200 (/)	250 (/)
GB50487-2008	100 (0)	185(0)
Strain rate	90 (10)	185 (0)
Crack rate	100 (0)	170 (8)
SPUC	100 (0)	185 (0)

6. Discussion and Perspective

6.1. Unloading Zonation Method

In this research, we summarize the commonly used methods for unloading zonation of large-scale rocky slopes and analyze the advantages and disadvantages of various methods. Considering that the physical phenomena of unloading are rebound loosening of existing cracks, shear dislocation of existing cracks, and new cracks in rock blocks, crack rate is added to characterize the crack development rate of the rock mass based on strain rate. To compensate for insufficient measurement of the rock mass structure when using the strain rate to divide the unloading zones and the insufficient measurement of the

strain rate when using the crack rate to divide the unloading zones, SPUC, which combines the crack rate and strain rate, is proposed to divide the unloading zones. The new method is applied to a large-scale rocky slope on the Qinghai–Tibet Plateau, that is, the JRS, and a series of conventional unloading zone division methods are used for verification. The results show that SPUC is feasible and accurate, its physical meaning is clear, and it can compensate for the defects of a single method.

The most widely used and mature indexes of unloading zone division in engineering are width of open cracks and number of open cracks. These indexes are used because they are easy to obtain in the field and these two indexes can directly characterize the characteristics of unloading. The threshold must be determined when using them to divide the unloading zones, which are not unified between projects (e.g., Table 2). Bao et al. [30] aimed to solve the problem that most indexes are not unified; strain rate with better uniformity in unloading zonation is proposed based on the statistical mechanics of rock masses, and the angle problem is discussed and proven based on the difference between the unloading direction and the actual adit survey trend. However, strain rate considers only the tensile displacement caused by unloading and is obviously insufficient to measure shear displacement (Figure 6a). Although using strain rate can also obtain good results because the unloading trend is basically the same when considering tensile displacement only and considering tensile and shear displacement simultaneously in most engineering projects, it is sometimes biased due to its insufficient measurement of the rock mass structure. Figure 7a shows that use of strain rate leads to demarcation of a strong unloading zone and weak unloading zone in the section with the same rock mass structure, i.e., the 80 m–100 m section. Thus, crack rate was introduced to consider the rock mass structure, which can adequately consider the contribution of closed cracks to the rock mass structure to compensate for the lack of strain rate in the characterization of shear displacement. However, use of crack rate leads to strain not being measured and cracks not being distinguished, which easily leads to the bottom boundary of the weak unloading zone being delineated at 170 m, and the slope of the curve after 170 m does not decrease but increases (Figure 7b). These are obviously unreasonable in the division of the unloading zones. When SPUC is used, these two problems can be avoided. The bottom boundary of the strong unloading zone is delineated as 100 m and the bottom boundary of the weak unloading zone is delineated as 185 m, which also corresponds well to Figure 5. In addition, SPUC is also based on field fracture investigation, which is easy to obtain and operate.

There are still some deficiencies when using SPUC in unloading zonation as follows. Our method showed improvement in determining how to characterize the rock mass quality because strain rate is not enough to measure this. Crack rate is added to characterize the rock mass quality, and SPUC is proposed to divide the unloading zones because of insufficient characterization of the rock mass quality by using strain rate. However, consideration of the rock mass quality is only based on the number of cracks. The size of the cracks and microcracks are not considered. This equivalence is somewhat similar to using RQD to measure rock mass quality. In addition, the horizontal depth of the adit that we used in this research is only 200 m, while the bottom of the weak unloading zone is close to 200 m; thus, the slope change in the curve in the weak unloading zone and the original rock stress area seems to not be significant. In addition, the proposal of an index still needs more cases for verification and one case in this research is not enough; more cases are needed to verify the accuracy of SPUC.

6.2. Unloading and Slope Evolution

Research on division of unloading zones is helpful for quality classification of the rock mass. It also helps to deepen understanding of the rock mass properties of the slope and provides the basis for later slope stability analysis and tunnel route selection.

Development of the unloading zone is a dynamic process with development of slope, and it controls the stability of the slope [11–13]. Stability of rock slopes is a dynamically

evolving geological historical process that is accompanied by aging deformation [5]. The dynamic process of its evolution has three typical stages, namely superficial transformation, aging deformation, and failure development [5]. These three stages have vertical zoning in the performance of the valley slope; that is, from the foot of the slope to the upper part of the slope, the three stages of superficial transformation, aging deformation, and failure development appear in sequence. Such spatial partitioning and dynamic changes over time are also accompanied by dynamic changes in the unloading zone.

With stress release in the process of valley incision, the rock mass undergoes rebound deformation to the free surface [51], and the stress field of the slope will be adjusted accordingly to adapt to the evolving deformation. Based on the research of geodynamic processes and stability control of high rock slope development in Southwest China, Huang [5] pointed out that downcutting of river valleys causes a hump-like stress distribution of the slope, including a stress reduction zone, stress increase zone, and original rock stress zone. Among them, the stress reduction zone and the stress increase zone correspond to the range of influence of rock mass unloading. Both the strong and weak unloading zones are within the stress reduction zone. The stress increase zone corresponds to the deep unloading zone (Figure 9) [5,20,21].

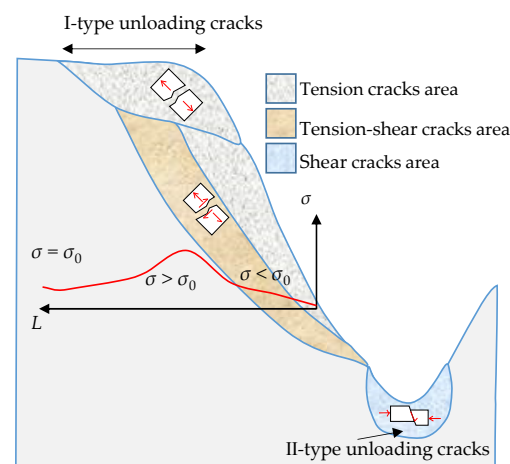


Figure 9. Stress distribution of valley slopes [5].

In the process of stress adjustment, to adapt to the new balance, the rock mass and its structure produce cracks or the old cracks develop further, resulting in changes in the rock mass structure and its properties, forming a similar underground chamber within a certain depth range of the valley slope. The unloading zone is the “loose circle” of the surrounding rock [53]. The distribution of the unloading zone is closely related to the slope stress field [21], and there are usually two types [59]. One is to characterize the range of the tensile stress area of the slope (corresponding to I-type unloading cracks, that is, the tensile-compressive stress area of the slope) (Figure 9), which is characterized by development of vertical unloading cracks in parallel slopes and generally occurs in the tensile-compressive stress combination area at a certain distance near the slope surface. The other is to characterize the range of the shear relaxation zone (corresponding to II-type unloading cracks, shear stress area of the slope), and its formation is directly related to the shear dislocation of the structural plane during the unloading process. The existence of II-type unloading cracks is also the main reason why this paper attempts to add crack ratio into strain rate to correct the division of the unloading zone. Strain rate cannot measure II-type shear unloading cracks that do not have an opening width, while the fracture rate index, which characterizes the quality of the rock mass, can cover the II-type shear unloading cracks, and the two can complement each other’s deficiencies.

7. Conclusions

Unloading controls the stability and safety of slope engineering. Therefore, it is of great importance to find a reliable unloading assessment. This paper proposes a method for quantitatively assessing slope unloading by combining a theoretical study with a case study. The conclusions are as follows.

1. Considering that unloading is the process of energy release, elastic deformation and strain failure are the essences of the unloading process of the rock mass and rebound loosening of existing cracks; shear dislocation of existing cracks and new cracks of rock mass are the physical phenomena of unloading. A method of dividing the unloading zone, SPUC, is proposed based on statistical rock mass mechanics and damage mechanics.
2. The Δh -SPUC curve regularly varies and can be divided into three parts according to the slopes of the curve. The slope unloading zone can be divided into strong and weak unloading zones. The extent of the strong and weak unloading zones can be determined by the two inflexions of the curve.
3. The unloading zonation method of SPUC is applied to a controlled slope of a railway, and a series of conventional unloading zone division methods are used for verification. The results show that the method is feasible and accurate, its physical meaning is clear, and it can compensate for the defect of using any single method.

Author Contributions: Conceptualization, Z.X., X.S. and G.C.; methodology, Z.X. and X.S.; investigation, Z.X. and Z.L.; writing—original draft preparation, Z.X. and X.S.; writing—review and editing, G.C.; visualization, X.Y. All authors have read and agreed to the published version of the manuscript.

Funding: This research was supported by the National Natural Science Foundation of China (Grant Nos. 41972284 and 42090054). This work was also supported by the State Key Laboratory of Geohazard Prevention and Geoenvironment Protection Independent Research Project (SKLGP2020Z005).

Institutional Review Board Statement: Not applicable.

Informed Consent Statement: Not applicable.

Data Availability Statement: The data presented in this study are available on request from the corresponding author.

Acknowledgments: The data of this work were provided to a large extent by Power China Chengdu Engineering Co., Ltd., and China Railway Eryuan Engineering Group Co., Ltd., to whom we extend our sincere thanks for the constructive cooperation. We would like to thank the anonymous reviewers who provided constructive reviews for improving this paper.

Conflicts of Interest: The authors declare no conflict of interest.

References

1. Ding, L.; Qasim, M.; Jadoon, I.A.; Khan, M.A.; Xu, Q.; Cai, F.; Wang, H.; Baral, U.; Yue, Y. The India–Asia collision in north Pakistan: Insight from the U–Pb detrital zircon provenance of Cenozoic foreland basin. *Earth Planet. Sci. Lett.* **2016**, *455*, 49–61. <https://doi.org/10.1016/j.epsl.2016.09.003>.
2. Ding, L.; Spicer, R.A.; Yang, J.; Xu, Q.; Cai, F.; Li, S.; Lai, Q.; Wang, H.; Spicer, T.E.V.; Yue, Y.; et al. Quantifying the rise of the Himalaya orogen and implications for the South Asian monsoon. *Geology* **2017**, *45*, 215–218. <https://doi.org/10.1130/g38583.1>.
3. Jiang, T.; Shen, Z.; Yang, M. A new model approach to predict the unloading rock slope displacement behavior based on monitoring data. *Struct. Eng. Mech.* **2018**, *67*, 105–113. <https://doi.org/10.12989/sem.2018.67.2.105>.
4. Ullah, J.; Luo, M.; Ashraf, U.; Pan, H.; Anees, A.; Li, D.; Ali, M.; Ali, J. Evaluation of the geothermal parameters to decipher the thermal structure of the upper crust of the Longmenshan fault zone derived from borehole data. *Geothermics* **2022**, *98*, 102268. <https://doi.org/10.1016/j.geothermics.2021.102268>.
5. Huang, R. Geodynamical process and stability control of high rock slope development. *Chin. J. Rock Mech. Eng.* **2008**, *27*, 1525–1544.
6. Tang, L.-Q.; Tang, K.; Nie, D.-X.; Wang, J.-J.; Liu, D.-Y. High slope stability of diversion power system intake of Jinchuan hydropower station. *J. Mt. Sci. Engl.* **2013**, *10*, 1109–1117. <https://doi.org/10.1007/s11629-013-2418-x>.

7. Chen, G.; Chen, T.; Chen, Y.; Huang, R.; Liu, M. A new method of predicting the prestress variations in anchored cables with excavation unloading destruction. *Eng. Geol.* **2018**, *241*, 109–120. <https://doi.org/10.1016/j.enggeo.2018.05.015>.
8. Wu, L.; Deng, H.; Huang, R.; Zhang, L.; Guo, X.; Zhou, Y. Evolution of Lakes Created by Landslide Dams and The Role of Dam Erosion: A Case Study of the Jiajun Landslide on the Dadu River, China. *Quat. Int.* **2019**, *503*, 41–50. <https://doi.org/10.1016/j.quaint.2018.08.001>.
9. Tu, G.; Deng, H.; Shang, Q.; Zhang, Y.; Luo, X. Effect of unloading in two directions on the formation of a deep-seated flexural toppling failure. *Int. J. Rock Mech. Min. Sci.* **2021**, *142*, 104790. <https://doi.org/10.1016/j.ijrmms.2021.104790>.
10. Si, X.; Li, X.; Gong, F.; Huang, L.; Liu, X. Experimental investigation of failure process and characteristics in circular tunnels under different stress states and internal unloading conditions. *Int. J. Rock Mech. Min. Sci.* **2022**, *154*, 105116. <https://doi.org/10.1016/j.ijrmms.2022.105116>.
11. Chen, H.; Tang, H.; He, X.; Zhao, X. Study on Failure Mechanism of Gongjiafang Bank Slope in Wu Gorge of the Three Gorges, the Yangtze River, China. *Front. Struct. Civ. Eng.* **2013**, *368–370 Pt 1–3*, 1794–1799. <https://doi.org/10.4028/www.scientific.net/AMM.368-370.1794>.
12. Wu, L.; Shao, G.; Huang, R.; He, Q. Overhanging Rock: Theoretical, Physical and Numerical Modeling. *Rock Mech. Rock Eng.* **2018**, *51*, 3585–3597. <https://doi.org/10.1007/s00603-018-1543-9>.
13. Wu, Y.; Lan, H. Landslide Analyst—A landslide propagation model considering block size heterogeneity. *Landslides* **2019**, *16*, 1107–1120. <https://doi.org/10.1007/s10346-019-01154-2>.
14. Qi, S.; Wu, F.; Yan, F.; Lan, H. Mechanism of deep cracks in the left bank slope of Jinping first stage hydropower station. *Eng. Geol.* **2004**, *73*, 129–144. <https://doi.org/10.1016/j.enggeo.2003.12.005>.
15. Zhu, L.; Cui, S.H.; Pei, X.J. Investigation of the characteristics and long-runout movement mechanisms of the Luanshibao landslide on the eastern margin of the Qinghai-Tibet Plateau. *Soil Dyn. Earthq. Eng.* **2022**, *153*, 107094. <https://doi.org/10.1016/j.soildyn.2021.107094>.
16. Shang, Y.; Yang, Z.; Li, L.; Liu, D.; Liao, Q.; Wang, Y. A super-large landslide in Tibet in 2000: Background, occurrence, disaster, and origin. *Geomorphology* **2003**, *54*, 225. [https://doi.org/10.1016/S0169-555X\(02\)00358-6](https://doi.org/10.1016/S0169-555X(02)00358-6).
17. Zheng, D.; Huang, R. Quantitative study on the classification of unloading zones of high slopes. In *Landslides and Engineered Slopes. From the Past to the Future, Two Volumes+ CD-ROM*; CRC Press: Boca Raton, FL, USA, 2008; pp. 1073–1076. <https://doi.org/10.1201/9780203885284-c137>.
18. Tu, G.X.; Deng, H. Unloading depth of rock masses and its relations with river downcutting in deep valleys in Southwest China. *Eng. Geol.* **2021**, *288*, 106161. <https://doi.org/10.1016/j.enggeo.2021.106161>.
19. GB 50487-2008; Code for Engineering Geological Investigation of Water Resources and Hydropower. Ministry of Water Conservancy and Hydropower Planning and Design Institute: Beijing, China, 2008.
20. Shen, J.; Zhang, J.L.; Xu, J.; Liao, R.; Chen, C. Testing of slope stress zones and its application to unloading zonation. *Chin. J. Geotech. Eng.* **2007**, *29*, 1423–1427.
21. Li, R.; Liu, T. Research of Bank Slope Stress Field and Quantitative Indicators of Unloading Zones Classification. *J. North China Univ. Water Resour. Hydropower* **2014**, *2*, 76–80.
22. Yang, H.; Zeng, Y.; Lan, Y.; Zhou, X. Analysis of the excavation damaged zone around a tunnel accounting for geostress and unloading. *Int. J. Rock Mech. Min. Sci.* **2014**, *69*, 59–66. <https://doi.org/10.1016/j.ijrmms.2014.03.003>.
23. Deere, D. Technical Description of Rock Cores for Engineering Purposes. *Rock Mech. Eng. Geol.* **1963**, *1*, 18–22.
24. Deere, D. Geological Considerations. In *Rock Mechanics in Engineering Practice*; Stagg, K.G., Zienkiewica, O.C., Eds.; Wiley: London, UK, 1968; pp. 1–20.
25. Merritt, A. *Engineering Classification for In-Situ Rock*; University of Illinois at Urbana: Champaign, IL, USA, 1968.
26. Wu, F.; Liu, J.; Liu, T.; Zhuang, H.; Yan, C. A method for assessment of excavation damaged zone (EDZ) of a rock mass and its application to a dam foundation case. *Eng. Geol.* **2009**, *104*, 254–262. <https://doi.org/10.1016/j.enggeo.2008.11.005>.
27. Perras, M.; Diederichs, M.S. Predicting excavation damage zone depths in brittle rocks. *J. Rock Mech. Geotech.* **2016**, *8*, 60–74. <https://doi.org/10.1016/j.jrmge.2015.11.004>.
28. Zhao, W.-H.; Frost, J.D.; Huang, R.-Q.; Yan, M.; Jin, L.-D. Distribution and quantitative zonation of unloading cracks at a proposed large hydropower station dam Site. *J. Mt. Sci. Engl.* **2017**, *14*, 2106–2121. <https://doi.org/10.1007/s11629-017-4431-y>.
29. Andreev, V.; Lavrova, L. Experience in studying technogenic unloading in construction pits. *Hydrotech. Constr.* **1984**, *18*, 70–74. <https://doi.org/10.1007/bf01433114>.
30. Bao, H.; Wu, F.; Xi, P.; Xu, J.; Liang, N.; Yan, C.; Xu, W.; Qi, Q. A new method for assessing slope unloading zones based on unloading strain. *Environ. Earth Sci.* **2020**, *79*, 350. <https://doi.org/10.1007/s12665-020-09077-1>.
31. Li, W.; Tong, K.; Dong, Z. Examining method of unloading zone and study of unload behavior for high slope. *J. Rock Mech. Eng.* **2001**, *A1*, 1669–1673.
32. Li, C.J.; Li, X.B.; Liang, L.S. Dynamic response of existing tunnel under cylindrical unloading wave. *Int. J. Rock Mech. Min. Sci.* **2020**, *131*, 104342. <https://doi.org/10.1016/j.ijrmms.2020.104342>.
33. Lesparre, N.; Gibert, D.; Nicollin, F.; Nussbaum, C.; Adler, A. Monitoring the excavation damaged zone by three-dimensional reconstruction of electrical resistivity. *Geophys. J. Int.* **2013**, *195*, 972–984. <https://doi.org/10.1093/gji/ggt282>.
34. Neuzil, C. Groundwater Flow in Low-Permeability Environments. *Water Resour. Res.* **1986**, *22*, 1163–1195. <https://doi.org/10.1029/WR022i008p01163>.

35. Louis, C. Determination of in situ hydraulic parameters in jointed rock. In Proceedings of the Second Congress on Rock Mechanics, Belgrade, Serbia, 21–26 September 1970; Volume 1, pp. 40–45.
36. Sun, Y.; Huang, R. Research on quantification index of rock mass in riverside unloading zone classification. *Chin. J. Rock Mech. Eng.* **2012**, *31* (Suppl. 2), 3942–3949.
37. Cho, W.J.; Kim, J.-S.; Lee, C.; Choi, H.-J. Gas permeability in the excavation damaged zone at KURT. *Eng. Geol.* **2013**, *164*, 222–229. <https://doi.org/10.1016/j.enggeo.2013.07.010>.
38. Sorokin, A.A. Experience in using air testing for studying jointing of rocks. *Hydrotech. Constr.* **1983**, *17*, 264–274. <https://doi.org/10.1007/bf01429045>.
39. Liu, H.; Li, T.; Shen, J.; Wang, L. The application of RaA testing technique on researching deep fracture belts in a rock slope. *Chin. J. Geol. Hazards Prev.* **2004**, *15*, 107–111.
40. Wang, X. Radon Anomaly Analysis of Engineering Slopes. *Adv. Mater. Res.* **2011**, 261–263, 1161–1166. <https://doi.org/10.4028/www.scientific.net/AMR.261-263.1161>.
41. Zhang, S.; Shi, Z.; Wang, G.; Yan, R.; Zhang, Z. Groundwater radon precursor anomalies identification by decision tree method. *Appl. Geochem.* **2020**, *121*, 104696. <https://doi.org/10.1016/j.apgeochem.2020.104696>.
42. Jiang, H. *The Rock Mass Structure Features and Its Control Seepage Mechanism of Longkaikou Hydroelectric Power Station Dam Base on Jinsha River*; Chengdu University of Technology: Chengdu, China, 2006.
43. Qi, S.W.; Wu, F.Q.; Zhuang, H.Z.; Liu, T.; Yan, C.G.; Chai, J.F. Characteristics of unloading fissures in dam's base of Xiaowan hydropower station. *J. Rock Mech. Eng.* **2008**, *A1*, 2907–2912.
44. Guo, J. *Quantification Study on Weathering and Unloading Zones of Rock Mass in Yangfanggou Hydropower Station on Yalong River*; Chengdu University of Technology: Chengdu, China, 2010.
45. Pang, B.; Zheng, D. Fuzzy comprehensive evaluation-based quantified study on classification of unloading zones of Emeishan basalt. *Water Resour. Hydropower Eng.* **2016**, *5*, 157–161. <https://doi.org/10.13928/j.cnki.wrahe.2016.05.037>
46. Qian, K. The character of weathering, classification of unloading zones and engineering geological for the basalt. *Sichuan Water Power* **1992**, *3*, 33–37.
47. Lu, H. Engineering geological exploration of high arch dam. *Hydropower Technol. Yunnan* **1995**, *4*, 4–15.
48. Ju, G. *Engineering Geology Study Onweathered & Unloaded Granite Rockmass in Incisedvalley of Yellow River Laxiwa Hydroelectric Station*; Chengdu University of Technology: Chengdu, China, 2002.
49. Chen, Q.; Nie, D.X.; Pan, S.Y.; He, Z.C.; Xie, K. A study of coefficient of permeability as a quantitative classification index for unloaded zones of rockmass. *Hydrogeol. Eng. Geol.* **2011**, *38*, 48–53. <https://doi.org/10.16030/j.cnki.issn.1000-3665.2011.04.004>.
50. Twidale, C. On the origin of sheet jointing. *Rock Mech. Rock Eng.* **1973**, *5*, 163–187. <https://doi.org/10.1007/bf01238046>.
51. Jarman, D. Large rock slope failures in the Highlands of Scotland: Characterisation, causes and spatial distribution. *Eng. Geol.* **2006**, *83*, 161–182. <https://doi.org/10.1016/j.enggeo.2005.06.030>.
52. Hencher, S.; Knipe, R. Development of rock joints with time and consequences for engineering. In Proceedings of the 11th Congress of the International Society for Rock Mechanics, Lisbon, Portugal, 9–13 July 2007; Volume 1, pp. 223–226.
53. Wakasa, S.; Matsuzaki, H.; Tanaka, Y.; Matsukura, Y. Estimation of episodic exfoliation rates of rock sheets on a granite dome in Korea from cosmogenic nuclide analysis. *Earth Surf. Process. Landf.* **2006**, *31*, 1246–1256. <https://doi.org/10.1002/esp.1328>.
54. Guo, C.B.; Wu, R.A.; Jiang, L.W.; Zhong, N.; Wang, Y.; Dong, W.; Zhang, Y.S.; Yang, Z.H.; Meng, W.; Li, X.; et al. Typical Geohazards and Engineering Geological Problems Along the Ya'an-Linzi Section of the Sichuan-Tibet Railway, China. *Geoscience* **2021**, *35*, 1–17. <https://doi.org/10.19657/j.geoscience.1000-8527.2021.023>.
55. Wu, F.; Wang, S.; Song, S.; Lv, J. Statistical Principles in Mechanics of Rock Masses. *Chin. Sci. Bull.* **1994**, *6*, 493–503.
56. Wu, F.; Wang, S. A stress-strain relation for jointed rock masses. *Int. J. Rock Mech. Min. Sci.* **2001**, *38*, 591–598. [https://doi.org/10.1016/s1365-1609\(01\)00027-2](https://doi.org/10.1016/s1365-1609(01)00027-2).
57. Sun, X.; Chen, G.; Huang, M.; Zhang, S.; Yang, J.; Ma, J. Method for analyzing the evolution characteristics of in-situ stress field considering rheology and degradation: A deeply incised valley in Qinghai-Tibet Plateau, case study. *Eng. Geol.* **2023**, *315*, 107029. doi.org/10.1016/j.enggeo.2023.107029.
58. Hua, X.; Liu, T.; Liu, J. A New Coefficient and Method to Appraise Tunnel Rock Mass Integrity. *J. Railw. Eng. Soc.* **2017**, *34*, 43–46+86.
59. Huang, R.; Lin, F.; Chen, D.J.; Wang, D.H. Formation mechanism of unloading fracture zone of high slopes and its engineering behaviors. *J. Eng. Geol.* **2001**, *9*, 227–232.

Disclaimer/Publisher's Note: The statements, opinions and data contained in all publications are solely those of the individual author(s) and contributor(s) and not of MDPI and/or the editor(s). MDPI and/or the editor(s) disclaim responsibility for any injury to people or property resulting from any ideas, methods, instructions or products referred to in the content.